© Universiti Tun Hussein Onn Malaysia Publisher's Office

IJIE

Journal homepage: http://penerbit.uthm.edu.my/ojs/index.php/ijie
ISSN : 2229-838X e-ISSN : 2600-7916

The International Journal of Integrated Engineering

Decoupling Control of a Disc-type Rotor Magnetic Bearing

Danh Huy Nguyen[1], Manh Linh Nguyen[1], Tung Lam Nguyen[1*]

[1]School of Electrical Engineering,
Hanoi University of Science and Technology, Hanoi, 100000, VIETNAM

*Corresponding Author

DOI: https://doi.org/10.30880/ijie.2021.13.05.027
Received 15 April 2020; Accepted 15 September 2021; Available online 24 November 2021

Abstract: A disc-type rotor magnetic bearing with 3-pole magnet is considered in the paper. The disc-type rotor supported by electro-magnetic forces has potential in industrial application especially in flywheel energy storage systems. However, coupling phenomenon in acting forces makes the balancing control problem in the system challenging. Based on analysing magnetic forces acting on the rotor, the coupling mechanism is identified, and a coordinate transformation is formulated to decouple acting forces. Thanks to the transformation, control design is straightforward for each control channel leading to simple and straightforward control design. The goal of the design is to keep the rotor at its desired equilibrium in the presence of disturbance and parameters variation. The goal can be achieved when the controller is designed in discrete-time domain based on the linearized model, then, the disturbance is compensated by employing the one step delay technique. The validity and robustness of the controller are verified by various numerical simulations in which original nonlinear model is used.

Keywords: Magnetic bearing, coordinate transformation, discrete current control, disc-type rotor

1. Introduction

Active Magnetic Bearing (AMB) uses electromagnetic force generated by electromagnets to move and suspend the rotor at a predefined position following that the mechanical contact and friction between rotor and stator are removed. The magnetic suspension based on AMB offers many advantages over the conventional bearings such as long life, higher rotating speed, no lubrication, etc. Hence, AMBs have been widely used in many applications such as turbine engine [1], agile satellite [2], and especially in the Flywheel Energy Storage System (FESS) [3, 4, 5].

Since the force generated by the AMB is a strong nonlinear function of the coil current and the air gap, the control design for the AMB system is quite complicated and pay a lot of attention. To deal with the nonlinearity of the AMB, the control design is normally categorized into two approaches. In the first approach, a linear model is derived from its nonlinear counterpart by doing Taylor expansion around an equilibrium point. Then, various well-known controllers such as state feedback [6], robust H∞ [7, 8], sliding mode control [9, 10, 11], backstepping control [12] are designed based on the linear transfer function or state space model. Additional solutions such as adaptive [12], neural network [10] are also employed to improve the robustness of the control system. In the second approach, the control design is carried out based on the nonlinear model directly. For examples, a nonlinear one-step predictive control is proposed in [13] to stabilize an AMB with predefined linear dynamics. In [14], the flatness-based control is employed in which the nonlinear design of current, voltage, and cascaded feedback laws is carried out to track a desired sufficiently differentiable reference trajectory. The nonlinear backstepping method is also used in [15], [16], and [17] to achieve global exponential position tracking. Several control methods proposed for the bearing system such as robust control, fuzzy, exact linearization can be listed in [18, 19, 20, 21, 22]. Recently, in the way of intelligent controls, intelligent-based controls are developed for active magnetic bearing such as neural network and iterative learning techniques [23,

*Corresponding author: lam.nguyentung@hust.edu.vn

24, 25] It is evident that research on the active magnetic bearing with disc-type rotor is not well-established, coupling mechanisms are properly handled.

Although most above-mentioned control methods give good result and are valuable to the AMB system, not many controllers designed in discrete-time domain which suits well the embedded control systems are achieved. Hence, this paper focuses on developing of a simple discrete-time control algorithm which can easily be installed in low-cost digital controllers. In advance, the proposed control method must be robust against the disturbance due to the fact that several parameters of the AMB such as the coil resistance, inductance and the mass of the rotor may be inaccurate. To achieve these goals, a linearized discrete-time state space model of the AMB which includes the errors caused by the parameter variation is built first. Then, a control law which fulfills a predefined position error dynamic is designed based on the predictive control technique. A control problem of a disc-type rotor magnetic bearing with 3-pole magnet is considered. The configuration exhibit strong couplings between the acting forces. The paper proposes a decoupling strategy based on a coordinate transformation to eliminate coupling effects; this property make the control design process easier. The transformation can be generalized to other disc-type rotors with different poles configuration. The validity of the proposed method is verified by various numerical simulations.

2. Mathematical Model of a Dual Coils Magnetic Actuator

A simple single coil magnetic actuator is shown in Fig. 1. In which, N is the number of the turns of the coil, I is the current, A_g is the cross section area and g is the air gap, l is the length of the magnetic circuit. The mathematical model of the magnetic actuator is based on the following assumptions:

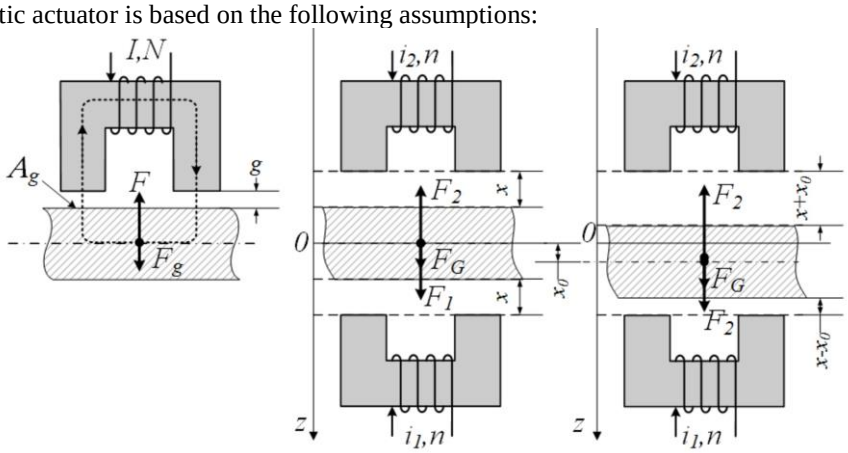

Fig. 1 - Single and dual coils magnetic actuator

Assumption 1: The permeability of the isotropic mediums used in the paper μ is constant in each segment, which results in:

$$B_j = \mu_j H_j \tag{1}$$

in which, B is the magnetic flux density, H is the magnetic field intensity and j is the index of the segment.

Assumption 2: The permeability of the air gap is much less than the permeability of the iron core, i.e., $\mu_g \ll \mu_c$

Applying the Ampere's loop law for the magnetic circuit, it gives

$$\sum_{j=1}^{N_s} H_j l_j = \sum_{j=1}^{N_s} B_j I_j \tag{2}$$

where N_s is the number of segments. In view of *Assumption 1*, (2) can be rewritten as

$$\sum_{j=1}^{N_s} \frac{B_j l_j}{\mu_j} = \sum_{j=1}^{N_s} B_j I_j \tag{3}$$

Because there are only two air gaps in the circuit and based on *Assumption 2*, a simple manipulation yields

$$B = \frac{\mu_g NI}{2g} \tag{4}$$

The energy, which is stored in the air gap, can be described by

$$E = A_g g \int H dB \tag{5}$$

Since H is a constant, it results in

$$E = A_g g H B \tag{6}$$

The electromagnetic force F is defined as

$$F = \frac{dE}{dg} \tag{7}$$

By using (1), (4) and (6), it can be deduced that

$$F = \frac{\mu_g N^2 A_g}{4}\left(\frac{I}{g}\right)^2 \tag{8}$$

In our application, a dual coils magnetic actuator is used as shown in Fig.1. The rotor is levitated and kept in the middle of the two cores by two opposite electromagnetic force F_1 and F_2. The influence of gravity is represented by F_g. In details,

$$F_1 = \frac{\mu_g N^2 A_g}{4}\left(\frac{i_1}{x_1}\right)^2 = \frac{K}{4}\left(\frac{i_1}{x_1}\right)^2 \tag{9}$$

$$F_2 = \frac{\mu_g N^2 A_g}{4}\left(\frac{i_2}{x_2}\right)^2 = \frac{K}{4}\left(\frac{i_2}{x_2}\right)^2 \tag{10}$$

where x_1, x_2 represent the two air gaps and $K = \mu_g N^2 A_g$. Denote the nominal air gap by x_0 and x is the deviation of the rotor from the nominal position, then it can be derived from Fig. 2 that

$$x_1 = x_0 - x, \quad x_2 = x_0 + x \tag{11}$$

By using Newton's law, the dynamic of the system is

$$m\ddot{x} = F_1 - F_2 + F_g \tag{12}$$

Assume that the two coils are identical, by applying Kirchoff's voltage law and take the back electromotive force caused by the air gap flux change into consideration, the voltage equation of each coil is

$$u_1 = Ri_1 + L_s \frac{di_1}{dt} + \frac{K}{2}\frac{d}{dt}\left(\frac{i_1}{x_1}\right) \tag{13}$$

$$u_2 = Ri_2 + L_s \frac{di_2}{dt} + \frac{K}{2}\frac{d}{dt}\left(\frac{i_2}{x_2}\right) \tag{14}$$

where L_s and R are the inductance and resistance of each coil, respectively. From (9)-(14), the nonlinear dynamic of the dual coils magnetic actuator can be represented by

$$\begin{cases} \dot{x} = \vartheta \\ \dot{\vartheta} = \dfrac{K}{4m}\left(\dfrac{i_1}{x_1}\right)^2 - \dfrac{K}{4m}\left(\dfrac{i_2}{x_2}\right)^2 + \dfrac{F_g}{m} \\ \dot{i}_1 = \dfrac{2x_1}{2L_s x_1 + K}\left(-Ri_1 - \dfrac{K}{2x_1^2}\vartheta i_1 + u_1\right) \\ \dot{i}_2 = \dfrac{2x_2}{2L_s x_2 + K}\left(-Ri_2 + \dfrac{K}{2x_2^2}\vartheta i_2 + u_2\right). \end{cases} \tag{15}$$

in which J is the velocity of the rotor. The dynamical model of the actuator specifies nonlinearity corresponding to current/air gap ratio.

3. Linearization of a Magnetic Actuator

As stated by the system equation (15), the dual coils magnetic actuator is quite complicated with four state variables and two control inputs. To simplify the system, the differential mode is chosen. In detail, denote the equilibrium point as $[\overline{x}, \overline{J}, \overline{i}_1, \overline{i}_2]$ corresponding to input voltage $[\overline{u}_1, \overline{u}_2]$, it yields

$$\begin{aligned} i_1 &= \overline{i}_1 + i, \qquad i_2 = \overline{i}_2 - i \\ u_1 &= \overline{u}_1 + u, \quad u_2 = \overline{u}_2 - u \end{aligned} \tag{16}$$

where i and u are the small deviations of the current from the equilibrium. Suppose that the magnetic actuator is always bias by a constant current I_b and the nominal position x_0 is chosen as the equilibrium, then by solving (15) in which all the differentials are zero, it results in

$$\begin{aligned} &\overline{x} = x_0, \quad \overline{J} = 0 \\ &\overline{i}_1 = I_b - \frac{F_g x_0^2}{KI_b}, \quad \overline{i}_2 = I_b + \frac{F_g x_0^2}{KI_b} \end{aligned} \tag{17}$$

Now, substitute (11) and (16) into (37), a simple manipulation gives

$$\dot{X} = \Phi(X, u) \tag{18}$$

where

$$\dot{X} = \begin{bmatrix} \dot{x} & \dot{\vartheta} & \dot{i} \end{bmatrix}^T \tag{19}$$

$$\mathsf{F}(X,u) = \begin{bmatrix} f_1(X,u) & f_2(X,u) & f_3(X,u) \end{bmatrix}^T \tag{20}$$

In details,

$$f_1(X,u) = \mathcal{J} \tag{21}$$

$$f_2(X,u) = \frac{K}{4m}\left(\frac{\bar{i}_1 + i}{x_0 - x}\right)^2 - \frac{K}{4m}\left(\frac{\bar{i}_1 - i}{x_0 + x}\right)^2 + \frac{F_g}{m} \tag{22}$$

$$\begin{aligned} f_3(X,u) = {} & \frac{(x_0 - x)}{2L_s(x_0 - x) + K}\left[-R(\bar{i}_1 + i) + (\bar{u}_1 + u)\right] \\ & - \frac{(x_0 - x)}{2L_s(x_0 - x) + K}\left[\frac{K}{2(x_0 - x)^2}\mathcal{J}\right](\bar{i}_1 + i) \\ & + \frac{(x_0 + x)}{2L_s(x_0 + x) + K}\left[-R(\bar{i}_2 - i) + (\bar{u}_2 - u)\right] \\ & - \frac{(x_0 + x)}{2L_s(x_0 + x) + K}\left[\frac{K}{2(x_0 + x)^2}\mathcal{J}\right](\bar{i}_2 - i) \end{aligned} \tag{23}$$

It would be seen that the original nonlinear system (37) of two inputs $\left[u_1, u_2\right]$ and four state variables $\left[x, \mathcal{J}, i_1, i_2\right]$ is now transformed into a nonlinear system (18) with only one input u and three state variables $\left[x, \mathcal{J}, i\right]$. Now, applying Taylor's expansion for the right hand side of (18) and neglect all the high order differential terms, i.e, higher than 1st order, it results in the following linear system

$$\begin{cases} \dot{X} = \mathbf{A}X + \mathbf{B}u + \mathbf{F} \\ y = \mathbf{C}X \end{cases} \tag{24}$$

in which

$$X = \begin{bmatrix} x & \mathcal{J} & i \end{bmatrix}^T, \quad y = \begin{bmatrix} x_k & i_k \end{bmatrix}^T \tag{25}$$

$$\mathbf{A} = \begin{bmatrix} 0 & 1 & 0 \\ \dfrac{K\left(\bar{i}_1^2 + \bar{i}_2^2\right)}{2mx_0^3} & 0 & \dfrac{K\left(\bar{i}_1 + \bar{i}_2\right)}{2mx_0^2} \\ 0 & -\dfrac{K\left(\bar{i}_1 + \bar{i}_2\right)}{4x_0^2(L_0 + L_s)} & -\dfrac{R}{L_0 + L_s} \end{bmatrix} \tag{26}$$

$$\mathbf{B} = \begin{bmatrix} 0 & 0 & \dfrac{1}{L_0 + L_s} \end{bmatrix}^T, \quad \mathbf{C} = \begin{bmatrix} 1 & 0 & 0 \\ 0 & 0 & 1 \end{bmatrix} \tag{27}$$

$$\mathbf{F} = \begin{bmatrix} 0 & \dfrac{F_g}{m} & 0 \end{bmatrix}^T, \quad L_0 = \frac{K}{2x_0} \tag{28}$$

In equation (24), X and u are regarded as the small deviation of state and control variables from the equilibrium. The linear model in that equation reflects the behavior of the magnetic actuator in a small vicinity around the equilibrium and can be used for control design.

4. Disc-type Three Phases Active Magnetic Bearing

In this section, mechanical and electrical transformations are introduced for the disc-type three phase active magnetic bearing. The transformations result in a decoupling structure that allow separately designing control channels.

4.1 Coordinate Transformation for Mechanical Signals

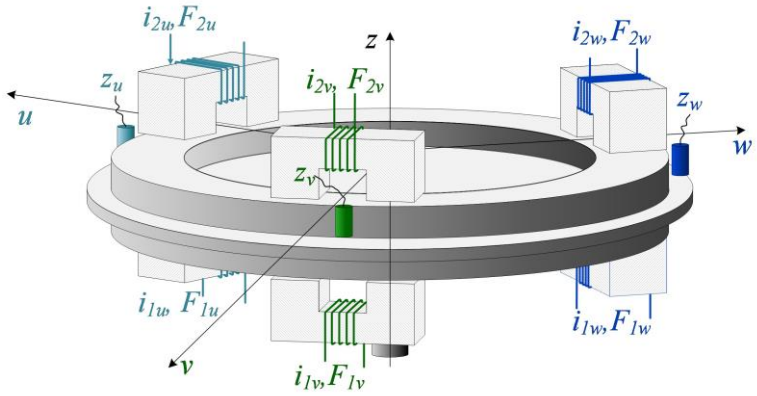

Fig. 2 - Physical configuration

In this research, a three-phase active magnetic bearing (3PAMB) which is used in flywheel energy storage system (FESS) is proposed. The configuration of the magnetic support disc-type flywheel is illustrated in Figure 2.

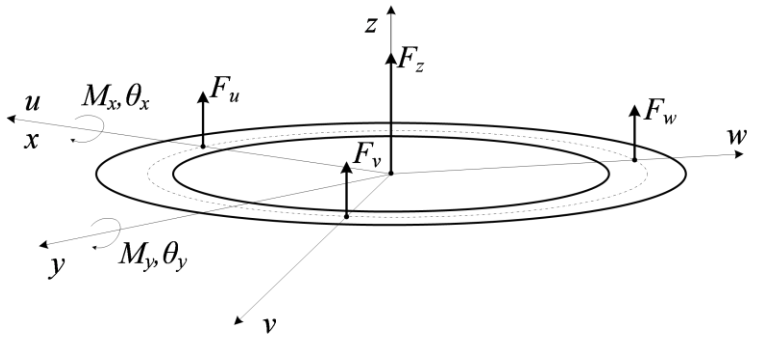

Fig. 3 - Co-ordinates representation

The system consists of three dual coils magnetic actuators distributed equally in space of rotor's periphery, corresponding to u, v, w phases and acting forces F_u, F_v, F_w resulting in u, v, and w displacements. The disc-type flywheel with its coordinate is depicted in Figure 3. Without loss of generality, $Oxyz$ coordinate is selected in such away the x and u axes are coincided. q_x and q_y are rotational angles about x and y axis. These forces are simultaneously controlled to suspend the rotor in the air gap. Motions perpendicular to z axis is assumed to be well stabilized by other magnetic actuators independently and not considered in control design. It should be noted that this assumption implying can only move vertically and rotate along x and y directions. The motion equation of the flywheel in $Oz q_x q_y$ coordinate is given as:

$$\mathbf{M}\begin{bmatrix} \ddot{z} \\ \ddot{\theta}_x \\ \ddot{\theta}_y \end{bmatrix} = \begin{bmatrix} m & 0 & 0 \\ 0 & J_x & 0 \\ 0 & 0 & J_y \end{bmatrix} \begin{bmatrix} \ddot{z} \\ \ddot{\theta}_x \\ \ddot{\theta}_y \end{bmatrix} = \begin{bmatrix} F_{ze} \\ M_{xe} \\ M_{ye} \end{bmatrix} - \begin{bmatrix} F_{zd} \\ M_{xd} \\ M_{yd} \end{bmatrix} \tag{29}$$

where m is the flywheel mass, J_x and J_y are the flywheel inertia in x and y directions. F_{ze}, M_{xe}, and M_{ye} are magnetic force and torques acting on z, x, and y axes, respectively. As well F_{zd}, M_{xd}, and M_{yd} are corresponding disturbances (29) characterizing independent motion in each direction, however this is not the actual

actuating and sensing system due to physical arrangement of the magnets and position sensors as shown in Figure 2.

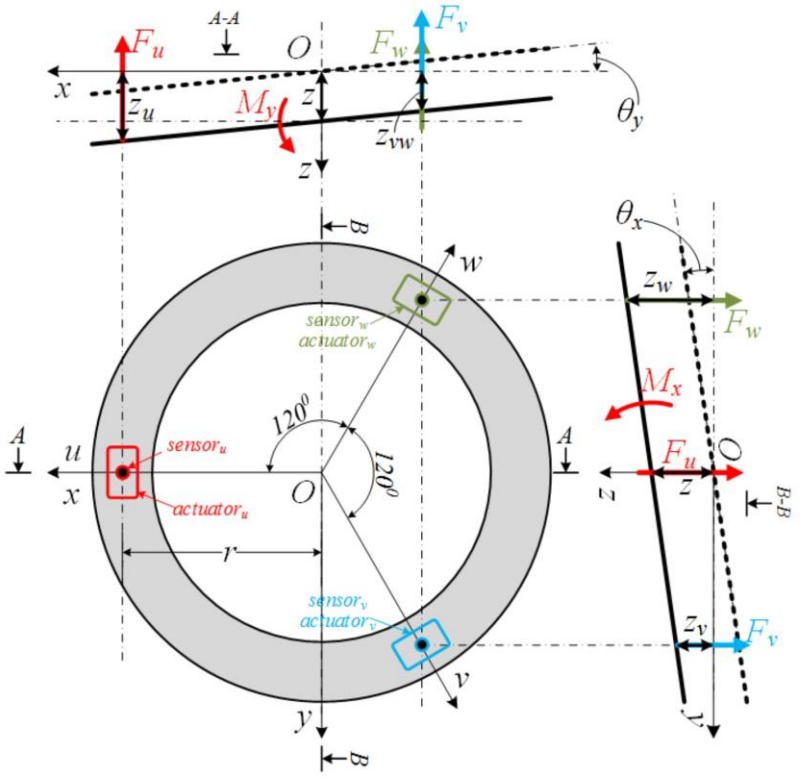

Fig. 4 - Force, torque, and position relationship between $Oxyz$ and $Oz\theta_x\theta_y$ coordinates

Figure 4 suggests that, after fundamental geometrical manipulations, the transformation from $Oxyz$ to $0zq_xq_y$ can be obtained as

$$\begin{bmatrix} z \\ q_x \\ q_y \end{bmatrix} = \begin{bmatrix} \frac{1}{3} & \frac{1}{3} & \frac{1}{3} \\ 0 & \frac{1}{r\sqrt{3}} & -\frac{1}{r\sqrt{3}} \\ \frac{2}{3r} & -\frac{1}{3r} & -\frac{1}{3r} \end{bmatrix} \begin{bmatrix} z_u \\ z_v \\ z_w \end{bmatrix} = \mathbf{S} \begin{bmatrix} z_u \\ z_v \\ z_w \end{bmatrix} \tag{30}$$

On the contrary, one can also derive the inverse transformation as

$$\begin{bmatrix} z_u \\ z_v \\ z_w \end{bmatrix} = \begin{bmatrix} 1 & 0 & r \\ 1 & -\frac{\sqrt{3}}{\sqrt{2}}r & -\frac{r}{2} \\ 1 & \frac{\sqrt{3}}{\sqrt{2}}r & -\frac{r}{2} \end{bmatrix} \begin{bmatrix} z \\ q_x \\ q_y \end{bmatrix} = \mathbf{S}^{-1} \begin{bmatrix} z \\ q_x \\ q_y \end{bmatrix} \tag{31}$$

In a similar fashion, magnetic forces F_u, F_v, and F_w are converted into axial force F_{ze}, torque M_{xe}, and M_{ye} about x and y axes, respectively.

$$\begin{bmatrix} F_{ze} \\ M_{xe} \\ M_{ye} \end{bmatrix} = \begin{bmatrix} 1 & 1 & 1 \\ 0 & \frac{\sqrt{3}}{2}r & -\frac{\sqrt{3}}{2}r \\ -r & \frac{r}{2} & \frac{r}{2} \end{bmatrix} \begin{bmatrix} F_u \\ F_v \\ F_w \end{bmatrix} = \mathbf{R} \begin{bmatrix} F_u \\ F_v \\ F_w \end{bmatrix} \tag{32}$$

From equations (29) and (32), it is straightforward to derive axial motions z_u, z_v, and z_w resulting from axial magnetic forces F_u, F_v, and F_w corresponding to disturbances F_{ud}, F_{vd}, and F_{wd} as follows

$$\begin{bmatrix} \ddot{z}_u \\ \ddot{z}_v \\ \ddot{z}_w \end{bmatrix} = \mathbf{S}^{-1} \begin{bmatrix} \ddot{z} \\ \ddot{\theta}_x \\ \ddot{\theta}_y \end{bmatrix} = \mathbf{S}^{-1}\mathbf{M}^{-1}\mathbf{R} \begin{bmatrix} F_u \\ F_v \\ F_w \end{bmatrix} - \mathbf{S}^{-1}\mathbf{M}^{-1}\mathbf{R} \begin{bmatrix} F_{ud} \\ F_{vd} \\ F_{wd} \end{bmatrix} \tag{33}$$

where the mass matrix is denoted by $\mathbf{H}$ and is defined as

$$\mathbf{H} = \mathbf{S}^{-1}\mathbf{M}^{-1}\mathbf{R}$$

$$= \begin{bmatrix} 1 & 0 & R \\ 1 & -\frac{\sqrt{3}}{2}r & -\frac{r}{2} \\ 1 & \frac{\sqrt{3}}{2}r & -\frac{r}{2} \end{bmatrix} \begin{bmatrix} \frac{1}{m} & 0 & 0 \\ 0 & \frac{1}{J_x} & 0 \\ 0 & 0 & \frac{1}{J_y} \end{bmatrix} \begin{bmatrix} 1 & 1 & 1 \\ 0 & \frac{\sqrt{3}}{2}r & -\frac{\sqrt{3}}{2}r \\ -r & \frac{r}{2} & \frac{r}{2} \end{bmatrix} \tag{34}$$

$$= \begin{bmatrix} h_{11} & h_{12} & h_{13} \\ h_{21} & h_{22} & h_{23} \\ h_{31} & h_{32} & h_{33} \end{bmatrix}$$

Equation (34) clearly show coupling mechanism between individual motions resulting in challenges in control design process. It is interesting to note that, the equation of motion described in equation(29) naturally characterized as decoupled motions in z, q_x, and q_y. From the observation, control design is carried for each decoupled individual motion in Ozq_xq_y coordinate and eventually, the control forces are transformed back to physical platform with three dual magnetic actuators.

4.2 Coordinate Transformation for Electrical Signals

The transformation in term of virtual acting force and torques F_{ze}, M_{xe}, and M_{ye} corresponding to virtual currents $i_{1,2z}$, $i_{i1,2x}$, and $i_{1,2y}$ is established. In order to proceed to design step we need the actual control i.e. current in each magnet in $Oxyz$. The arrangement of three upper magnets in $Oxyz$ and Ozq_zq_y are depicted as follows.

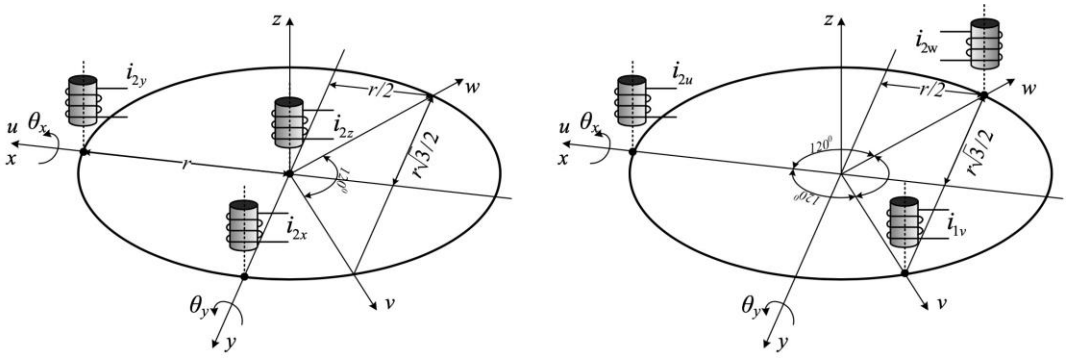

Fig. 5 - Current relationship between $Oxyz$ and $Oz\theta_x\theta_y$ coordinates

The virtual magnets in $Oz q_z q_y$ demonstrate that control input $i_{1,2z}$ is in charge of levitating the disc in z direction, $i_{i1,2x}$, and $i_{1,2y}$ produce torque to rotate the rotor along y and x directions, respectively. In order to derive the current transform, since dual-magnet systems are used, at first, we consider the upper-magnet group. As shown in Fig 5, we can derive the following relationship between virtual and actual control current

$$\begin{bmatrix} i_{2z} \\ i_{2x} \\ i_{2y} \end{bmatrix} = \begin{bmatrix} 1 & 1 & 1 \\ 0 & \frac{\sqrt{3}}{2} & -\frac{\sqrt{3}}{2} \\ -1 & \frac{1}{2} & \frac{1}{2} \end{bmatrix} \begin{bmatrix} i_{2u} \\ i_{2v} \\ i_{2w} \end{bmatrix} = \mathbf{E} \begin{bmatrix} i_{2u} \\ i_{2v} \\ i_{2w} \end{bmatrix} \tag{35}$$

in the same fashion we can derive the transformation for lower magnets

$$\begin{bmatrix} i_{1z} \\ i_{1x} \\ i_{1y} \end{bmatrix} = \begin{bmatrix} 1 & 1 & 1 \\ 0 & \frac{\sqrt{3}}{2} & -\frac{\sqrt{3}}{2} \\ -1 & \frac{1}{2} & \frac{1}{2} \end{bmatrix} \begin{bmatrix} i_{1u} \\ i_{1v} \\ i_{1w} \end{bmatrix} = \mathbf{E} \begin{bmatrix} i_{1u} \\ i_{1v} \\ i_{1w} \end{bmatrix} \tag{36}$$

4.3 Decoupling Control Structure

From the above-mentioned coordinate transformation, the decoupling control structure can be summarized in Figure 6.

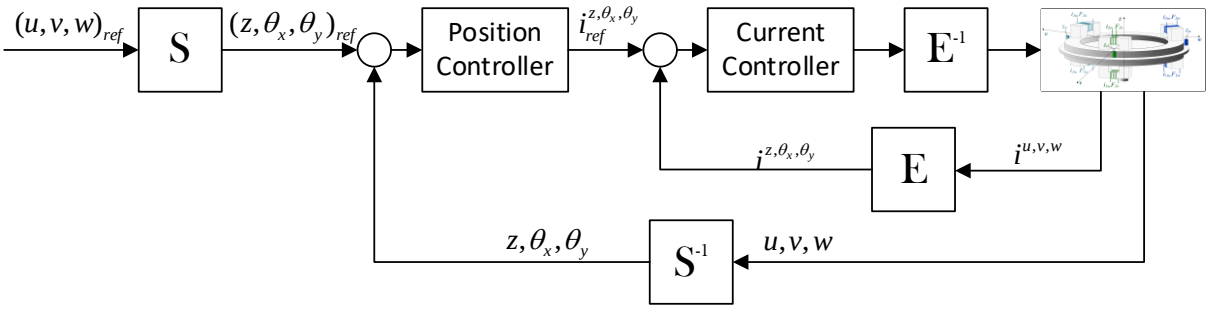

Fig. 6 - Control structure

The aforementioned coordinate transformations result in the following relationship

$$\begin{cases} F_{ze} = F_{1z} - F_{2z} = \dfrac{K}{4}\dfrac{i_{1z}^2}{(e-z)^2} - \dfrac{K}{4}\dfrac{i_{1z}^2}{(e+z)^2} \\ M_{xe} = (F_{1x} - F_{2x})r = \dfrac{K}{4}\dfrac{ri_{1z}^2}{(e-q_x r)^2} - \dfrac{K}{4}\dfrac{ri_{1z}^2}{(e+q_x r)^2} \\ M_{ye} = (F_{1y} - F_{2y})r = \dfrac{K}{4}\dfrac{ri_{1y}^2}{(e-q_y r)^2} - \dfrac{K}{4}\dfrac{ri_{2y}^2}{(e+q_y r)^2} \end{cases} \tag{37}$$

By using this proposed representation, the coupling effect is completely removed. The control design can be carried out for each channel independently. Then, the virtual control signals are transformed into the actual ones by a simple transformation. The control design for each independent actuator is carried out in the following section.

5. Control Design

Inheriting the decoupling scheme in section 4, the control problem of the disc-type rotor supported by the three-phase magnetic bearing can be transferred to a single dual-magnet. For control design purpose, a discrete time state-space model derived from (24) is used:

$$\begin{cases} X_{k+1} = \Phi X_k + \Gamma u_k + \mathbf{E} + \mathbf{d}_k \\ y_k = \mathbf{C} X_k \end{cases} \tag{38}$$

where T_s is the sampling time, $O(T_s)$ is the small error caused by the numerical approximation. The corresponding state-space variables and matrices of the discrete-time system equations (38) are as follows:

$$X_k = \begin{bmatrix} x_k & J_k & i_k \end{bmatrix}^T \tag{39}$$

$$\Phi = e^{\mathbf{A}T_s} = \begin{bmatrix} f_{11} & f_{12} & 0 \\ f_{21} & f_{22} & f_{23} \\ f_{31} & f_{32} & f_{33} \end{bmatrix} \tag{40}$$

$$\Gamma = \int_0^{T_s} e^{At}\,dt\,\mathbf{B} = \mathbf{A}^{-1}(\Phi - \mathbf{I}_3)\mathbf{B} = \begin{bmatrix} 0 & 0 & \Gamma_{31} \end{bmatrix}^T \tag{41}$$

$$\mathbf{E} = \int_0^{T_s} e^{At}\,dt\,\mathbf{F} = \mathbf{A}^{-1}(\Phi - \mathbf{I}_3)\mathbf{F} = \begin{bmatrix} 0 & E_{21} & 0 \end{bmatrix}^T \tag{42}$$

$$\mathbf{d}_k = \begin{bmatrix} 0 & d_{J,k} & d_{i,k} \end{bmatrix}^T \tag{43}$$

where $\mathbf{I}_3$ is an unity (3×3) matrix and $\mathbf{d}_k$ represents the error caused by the parameters variations.

5.1 Current Controller

From equation (38), the predictive current can be described by

$$i_{k+1} = f_{31}x_k + f_{32}J_k + f_{33}i_k + G_{31}u_k + d_{i,k} \tag{44}$$

Denote the desired current and the one step ahead current error by $i_{d,k}$ and $e_{i,k+1}$, respectively. In detail we have,

$$e_{i,k+1} = i_{d,k+1} - i_{k+1} \tag{45}$$

The control signal u_k which forces $e_{i,k+1}$ to zero can be obtained by solving the following equation

$$e_{i,k+1} = 0 \tag{46}$$

By substituting (44) into (46), a fundamental operation yields

$$u_k = \frac{1}{G_{31}}\left(i_{d,k+1} - f_{31}x_k - f_{32}J_k - f_{33}i_k - d_{i,k}\right) \tag{47}$$

Since $d_{i,k}$ is unknown, its corresponding approximation $\hat{d}_{i,k}$ is employed, instead. This approximation is based on the following assumption:

Assumption 3: The disturbance $d_i(t)$ is slow time-varying in comparison with the sampling frequency such that the difference between two consecutive sampling cycle is restricted by

$$d_{i,k} - d_{i,k-1} = O(T_s) \tag{48}$$

Based on (48) and (45), it gives

$$\hat{d}_{i,k} \approx d_{i,k-1} = i_k - f_{31}x_{k-1} - f_{32}J_{k-1} - f_{33}i_{k-1} - G_{31}u_{k-1} \tag{49}$$

As a result, the control action for the current loop is

$$u_k = \frac{1}{G_{31}}\left(i_{d,k+1} - f_{31}x_k - f_{32}J_k - f_{33}i_k - \hat{d}_{i,k}\right) \tag{50}$$

following that $e_{i,k} \to O(T_s)$ in one step.

5.2 Position Controller

Define the generalized predictive position error $E_{x,k+3}$ as

$$E_{x,k+3} = e_{x,k+3} + b_1 e_{x,k+2} + b_2 e_{x,k+1} + b_3 e_{x,k} \tag{51}$$

where b_1, b_2 and b_3 are design parameters which can be chosen such that (51) is Hurwitz, and $e_{x,k}$ is the instantaneous position error computed by

$$e_{x,k} = x_{d,k} - x_k \tag{52}$$

Based on (38), a fundamental operation gives

$$\begin{aligned} E_{x,k+3} = {} & g_{1,k+3} + (g_2 f_{11} + g_3 f_{21})x_k + (g_2 f_{12} + g_3 f_{22})J_k \\ & + g_3 f_{23} i_k + (g_3 E_{21} + g_4) - f_{12} f_{23} i_{k+1} + (g_3 - f_{12})d_{x,k} \end{aligned} \tag{53}$$

in which,

$$g_{1,k+3} = x_{d,k+3} + b_1 x_{d,k+2} + b_2 x_{d,k+1} + b_3 e_{x,k}, \quad g_2 = -\left(f_{11}^2 + f_{12} f_{21} + b_1 f_{11} + b_2\right) \tag{54}$$

$$g_3 = -\left(f_{11} f_{12} + f_{12} f_{22} + b_1 f_{12}\right), \quad g_4 = -f_{12} E_{21} \tag{55}$$

The command current which forces the generalized position error to zero is obtained by solving

$$E_{x,k+3} = 0 \tag{56}$$

which results in

$$i_{d,k+1} = \frac{g_{1,k+3} + q_1 x_k + q_2 J_k + q_3 i_k + q_4 + (g_3 - f_{12}) d_{x,k}}{f_{12} f_{23}} \tag{57}$$

with

$$\begin{aligned} q_1 &= g_2 f_{11} + g_3 f_{21}, \quad q_2 = g_2 f_{12} + g_3 f_{22} \\ q_3 &= g_3 f_{23}, \qquad\quad q_4 = g_3 E_{21} + g_4 \end{aligned} \tag{58}$$

Again, the estimation of the unknown terms $d_{x,k}$ is based on (38) and the one step delay technique as following

$$\begin{aligned} \hat{d}_{x,k} &\approx d_{x,k-1} \\ &= J_k - f_{21} x_{k-1} - f_{22} J_{k-1} - E_{21} \end{aligned} \tag{59}$$

We define

$$\tilde{d}_{x,k} = d_{x,k} - \hat{d}_{x,k} \tag{60}$$

and assume that the sampling frequency is sufficient large such that

$$\tilde{d}_{x,k} = O(T_s) \tag{61}$$

Then, the following command current can drive the rotor to its desired position with $O(T_s)$ error despite the parameters variation

$$i_{d,k+1} = \frac{g_{1,k+3} + q_1 x_k + q_2 J_k + q_3 i_k + q_4 + (g_3 - f_{12}) \hat{d}_{x,k}}{f_{12} f_{23}} \tag{62}$$

6. Simulation Results

To evaluate the feasibility and effectiveness of the control method, numerical simulations are carried out in this section. The parameters of the magnetic actuator are provided in Table. 1 and proposed controller parameters $b_1 = -1.5$, $b_2 = 0.71$, $b_3 = -0.105$, and $T_s = 1$ ms. Initially, $u(t_0) = v(t_0) = w(t_0) = 0$, since the rotor is symmetrical and three electrical magnets are identical, it implies that dynamical responses of three magnets are analogous.

Table 1 - Parameters of the magnetic actuators

R_s	0.97	Ω
L_s	0.0542	mH
N	280	Rounds
x_0	0.001	m
A_g	0.0022	m2
m	14	kg
μ_g	1.2566×10−6	H/m

However, the final goal of the design is to stabilize the original nonlinear system around the equilibrium. Hence, various simulations with the nonlinear model are conducted in this section. The initial position of the rotor is $[u,v,w]=[-0.5\text{ mm},\ -0.34\text{ mm},\ 0.1\text{ mm}]$. At simulation time corresponding to sampling cycle 300^{th}, we introduce external noises of 1 Nm, 2 Nm, and 20 N to q_x, q_y, and z directions, respectively. The step responses of the control system are shown in Fig. 7. As can be observed, the system is stable without steady-state error after 70 sampling cycles. The overshoot is observed but well maintained in within the nomial airgap. The coil currents converge to their corresponding equilibriums. However, the oscillation always occurs in the transient state due to the fact that the desired controller only performs well in the vicinity of the equilibrium.

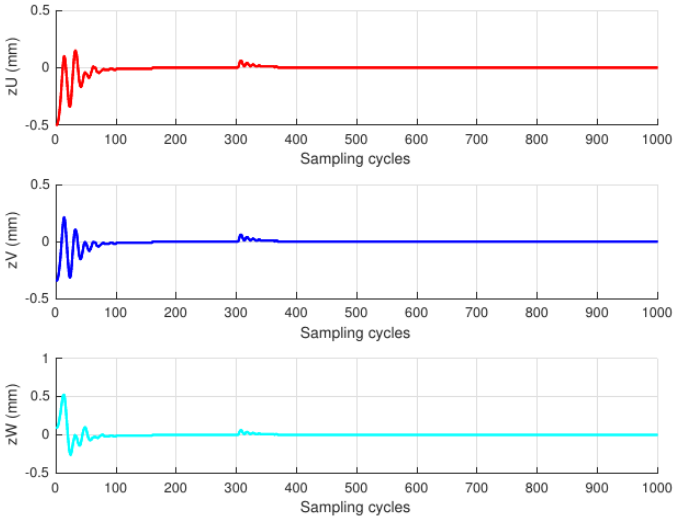

Fig. 7: Step responses of the controlled system

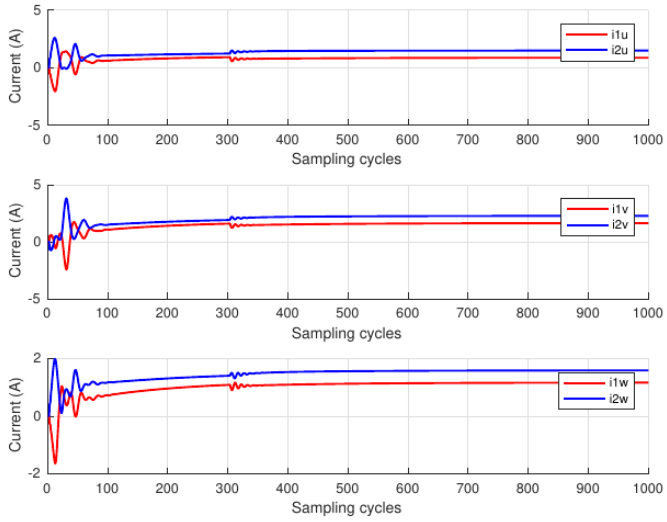

Fig. 8 - Control current responses

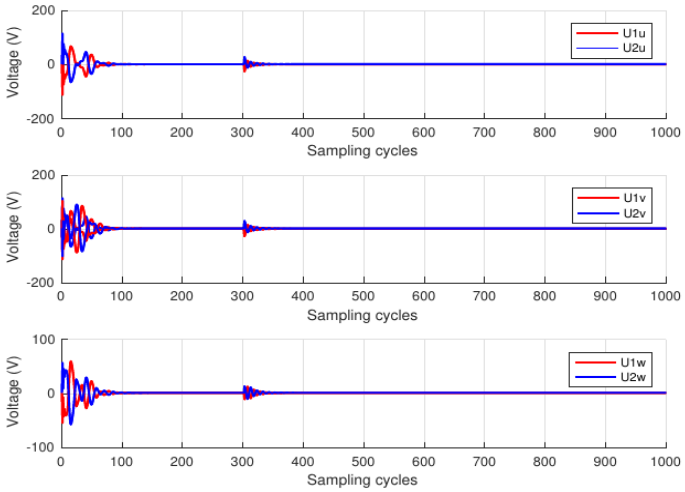

Fig. 9 - Control voltage responses

In general, the transient period in position responses is approximately of 0.1 s. The robustness of the controller is also verified by changing the rotor mass suddenly in the simulation. The result in Fig. 7 shows that the rotor quickly returns to its desired position in finite sampling cycles. Figure 8 indicates control currents corresponding to magnetic forces produced by the opposing magnets where it is witnessed the increase in control currents after sampling cycle 300^{th} to counteract the external disturbances. The applied control voltage, which is well maintained around 100 V, is presented in Fig. 9 implying the control input is of applicable range.

7. Conclusions

The contribution of the paper is the formulation of the coordinate transformation to decouple acting electromagnetic forces on the disc-type rotor. Based on the decoupling nature, control design can be done for each virtual electrical magnet independently and then the result is transformed back to actual actuators. In this research, the discrete time control design for the dual coil magnetic actuator applied to flywheel energy storage is discussed. First, the controller is designed based on the linearized model. Then, disturbance estimation technique is employed to enhance the robustness of the control system against the parameters variation. The effectiveness of the proposed controller is confirmed by various numerical simulations. The developed control design is straightforward and simple, the simulation results show good stabilizing ability of the controlled system. In the near future, we will look at the effects of rotational motion to the system and how the control can deal with this type of coupling. In addition, experimental works will be carried out in the next phase of our study.

Acknowledgement

This research is funded by the Hanoi University of Science and Technology (HUST) under project number T2021-PC-001.

References

[1] E. A. Knoth and J. P. Barber. (1998). Magnetic repulsion bearings for turbine engines. IEEE Transactions on Magnetics, vol. 24, no. 6, pp. 3141-3143. doi: 10.1109/20.92361

[2] H. Bangcheng, Z. Shiqiang, W. Xi and Y. Qian. (2012). Integral Design and Analysis of Passive Magnetic Bearing and Active Radial Magnetic Bearing for Agile Satellite Application. IEEE Transactions on Magnetics, vol. 48, no. 6, pp. 1959-1966. doi: 10.1109/TMAG.2011.2180731

[3] S.M. Mousavi G, Faramarz Faraji, Abbas Majazi, and Kamal Al-Haddad. (2017). A comprehensive review of Flywheel Energy Storage System technology. Renewable and Sustainable Energy Reviews, Volume 67, 2017, Pages 477-490, ISSN 1364-0321, https://doi.org/10.1016/j.rser.2016.09.060

[4] M. A. Awadallah and B. Venkatesh. (2015). Energy Storage in Flywheels: An Overview, Canadian Journal of Elec- trical and Computer Engineering, vol. 38, no. 2, pp. 183-193. doi: 10.1109/CJECE.2015.2420995

[5] A.A. Khodadoost Arani, H. Karami, G.B. Gharehpetian, and M.S.A. Hejazi. (2017). Review of Flywheel Energy Storage Systems structures and applications in power systems and microgrids. Renewable and Sustainable Energy Reviews, Volume 69, Pages 9-18, ISSN 1364-0321, https://doi.org/10.1016/j.rser.2016.11.166

[6] T. Mizuno, K. Araki and H. Bleuler. (1996). Stability analysis of self-sensing magnetic bearing controllers. IEEE

Transactions on Control Systems Technology, vol. 4, no. 5, pp. 572-579. doi: 10.1109/87.531923
[7] Guang-Ren Duan, Zhan-Yuan Wu, Chris Bingham and David Howe. (2000). Robust magnetic bearing control using stabilizing dynamical compensators. IEEE Transactions on Industry Applications, vol. 36, no. 6, pp. 1654-1660, Nov.-Dec. doi: 10.1109/28.887218
[8] Guang-Ren Duan and D. Howe. (2003). Robust magnetic bearing control via eigenstructure assignment dynamical compensation. IEEE Transactions on Control Systems Technology, vol. 11, no. 2, pp. 204-215. doi: 10.1109/TCST.2003.809253
[9] H. B. Oza, V. Thakar and B. Bandyopadhyay. (2010). Discrete time sliding mode control with application to magnetic levitation system. 2010 11th International Workshop on Variable Structure Systems (VSS), Mexico City, pp. 331-336. doi: 10.1109/VSS.2010.5544659
[10] Faa-Jeng Lin, Syuan-Yi Chen, Ming-Shi Huang. (2011). Adaptive complementary sliding-mode control for thrust active magnetic bearing system. Control Engineering Practice, Volume 19, Issue 7, Pages 711-722, ISSN 0967-0661, https://doi.org/10.1016/j.conengprac.2011.03.006
[11] Huynh V.V., Tsai YW. (2018). PI Sliding Mode Control for Active Magnetic Bearings in Flywheel. In: Duy V., Dao T., Zelinka I., Kim S., Phuong T. (eds) AETA 2017 - *Recent Advances in Electrical Engineering and Related Sciences: Theory and Application*
[12] Lili Dong and Silu You. (2014). Adaptive control of an active magnetic bearing with external disturbance. ISA Transactions, Volume 53, Issue 5, Pages 1410-1419, ISSN 0019-0578
[13] St´ephane Bonnet, J´erˆome De Miras, Borislav Vidolov. (2008). Nonlinear One-Step Predictive Control of an Active Magnetic Bearing. IFAC Proceedings, Volume 41, Issue 2, Pages 12183-12188, ISSN 1474-6670, ISBN 9783902661005
[14] J. Levine, J. Lottin and J. -. Ponsart. (1996). A nonlinear approach to the control of magnetic bearings. IEEE Transactions on Control Systems Technology, vol. 4, no. 5, pp. 524-544. doi: 10.1109/87.531919
[15] M. S. de Queiroz and D. M. Dawson. (1996). Nonlinear control of active magnetic bearings: a backstepping approach. IEEE Transactions on Control Systems Technology, vol. 4, no. 5, pp. 545-552. doi: 10.1109/87.531920
[16] D. H. Nguyen, T. L. Nguyen, M. L. Nguyen, and H. P. Nguyen. (2019). Nonlinear Control of an Active Magnetic Bearing with Output Constraint. International Journal of Power Electronics and Drive Systems, vol. 8, no. 5, p. 3666
[17] D. H. Nguyen, T. L. Nguyen, and D. C. Hoang. (2020). A non-linear control method for active magnetic bearings uith bounded input and output. Int. J. Electr. Comput. Eng., vol. 11, no. 4, pp. 2154-2164
[18] H. Du, N. Zhang, J. C. Ji, and W. Gao. (2010). Robust Fuzzy Control of an Active Magnetic Bearing Subject to Voltage Saturation. IEEE Trans. Control Syst. Technol., vol. 18, no. 1, pp. 164-169
[19] C. T. Hsu and S. L. Chen. (2002). Exact linearization of a voltage-controlled 3-pole active magnetic bearing system. IEEE Trans. Control Syst. Technol., vol. 10, no. 4, pp. 618-625
[20] M. S. Kang, J. Lyou, and J. K. Lee. (2010) Sliding mode control for an active magnetic bearing system subject to base motion. Mechatronics, vol. 20, no. 1, pp. 171-178
[21] A. Noshadi, J. Shi, W. S. Lee, P. Shi, and A. Kalam. (2017). Robust control of an active magnetic bearing system using H-infinity and disturbance observer-based control. J. Vib. Control, vol. 23, no. 11, pp. 1857-1870
[22] G. Kumar, M. D. Choudhury, S. Natesan, and K. Kalita. (2016) Design and Analysis of a Radial Active Magnetic Bearing for Vibration Control. Procedia Eng., vol. 144, pp. 810-816
[23] B. T. Costic, M. S. de Queiroz and D. N. Dawson. (2000). A new learning control approach to the active magnetic bearing benchmark system. Proceedings of the 2000 American Control Conference. ACC (IEEE Cat. No.00CH36334), pp. 2639-2643 vol.4, doi: 10.1109/ACC.2000.878684
[24] Lukasz Hladowski, Arkadiusz Mystkowski, Krzysztof Galkowski, Eric Rogers, Bing Chu. (2020) Application of the Dynamic Iterative Learning Control to the Heteroplanar Active Magnetic Bearing. IFAC-PapersOnLine, vol. 53, no. 2, pp. 1511-1516
[25] Z. Cao *et al.*, (2019). Sliding Mode Control with Neural Network for Active Magnetic Bearing System. IECON 2019 - 45th Annual Conference of the IEEE Industrial Electronics Society, pp. 744-749, doi.1109/IECON.2019.8926808